International Journal of Low-Carbon Technologies, 2025, **20**, 940–956
https://doi.org/10.1093/ijlct/ctae142
Original Article

OXFORD

Energetic, exergetic, environmental, and economic—4E analysis of an absorption refrigeration system operated by parabolic trough collectors

Álvaro Arteaga Díaz[1], Gaylord Enrique Carrillo Caballero[1], Yulineth Cárdenas Escorcia[2,*], Mohammad Hossein Ahmadi[3,*], Mohsen Sharifpur[4,5,*], Eric Alberto Ocampo Batlle[6], Edson Da Costa Bortoni[6]

[1]Grupo de Investigación EOLITO, Universidad Tecnológica de Bolívar (UTB), Cartagena 130002, Colombia
[2]Grupo de Investigación GIOPEN, Energy Department, Universidad de la Costa (CUC), Barranquilla 080016, Colombia
[3]Faculty of Mechanical Engineering, Shahrood University of Technology, Shahrood 3614773955, Iran
[4]School of Mechanical, Industrial and Aeronautical Engineering, University of the Witwatersrand, Private Bag 3, Wits 2050, Johannesburg 2001, South Africa
[5]Department of Medical Research, China Medical University Hospital, China Medical University, Taichung 404332, Taiwan
[6]Excellence Center in Renewable Energy and Energy Efficiency—EXCEN, Federal University of Itajubá—UNIFEI, Itajubá 37500-000, Brazil
*Corresponding authors. Faculty of Mechanical Engineering, Shahrood University of Technology, Shahrood 3614773955, Iran.
Email: mohammadhosein.ahmadi@gmail.com; Email: mohsen.sharifpur@up.ac.za; Grupo de Investigación GIOPEN, Energy Department, Universidad de la Costa (CUC), Barranquilla 080016, Colombia. Email: ycadena6@cuc.edu.co

Abstract

In search of ensuring the sustainability of current processes and the mitigation of the issues related to the high consumption of fossil fuels, different sectors of the global economy have decided to employ alternative methods and technologies to meet the demand and energy needs in their different applications and end uses. Among these end uses, cooling systems stand out, specifically in absorption or adsorption systems, where a thermal energy source is required for the operation of this type of system. At present, natural gas is mainly used worldwide as fuel for this type of process. As a result of the operation of this type of systems, in addition to the consumption of fossil fuel, an environmental impact generated by the pollutants produced in the combustion of natural gas is obtained. For this study, we developed the analysis of function of an absorption refrigeration system coupled to a parabolic trough system working with different heat transfer fluids (HTFs) as an option to replace the consumption of natural gas and the effect generated on the environment. For the development of this study, first, the opto-geometric model of the collector system was developed, with the purpose of determining the thermal behavior. Afterward, the operation of the refrigeration system was characterized in order to complete the energy states in each component of the system. With these models, the exergy levels and components with the highest energy destruction in each system were determined. Finally, the solar field configuration was determined to supply the thermal energy required by an absorption system installed at the Universidad Tecnológica de Bolivar (UTB) and thus the environmental impacts generated by the operation of the cooling system in the actual configuration of the UTB. From the results obtained, it was determined that for the parabolic trough collectors, the efficiencies are around 70%; for temperatures of 100°C, the exergy efficiency is 12%. For the different HTFs, water and supercritical CO_2 presented the best efficiencies for the evaluated conditions of the cooling system, which was defined for a cooling load capacity of 369.3 kW, which corresponds to the absorption cooling system of the UTB Auditorium.

Keywords: renewable energy; solar energy; parabolic trough collectors; refrigeration systems; absorption systems; exergy; exergy destruction; carbon footprint; emission calculation

1 Introduction

In search of ensuring the sustainability of current processes and the mitigation of the issues related to the high consumption of fossil fuels, different sectors of the global economy have decided to employ alternative methods and technologies to meet the demand and energy needs in their different applications and end uses. Among these end uses, cooling systems stand out, specifically in absorption or adsorption systems, where a thermal energy source is required for the operation of this type of system. At present, natural gas is mainly used worldwide as fuel for this type of process. As a result of the operation of this type of systems, in addition to the consumption of fossil fuel, an environmental impact generated by the pollutants produced in the combustion of natural gas is obtained [1]. This factor has motivated research studies on the use of renewable energies in air conditioning and refrigeration applications. In addition, the growing population rate has led to increased demands for indoor comfort, and higher standards of living are causing an ever-increasing demand for air conditioning around the world [2, 3]. According to the International Institute of Refrigeration, 15% of total produced electricity is used to meet indoor air conditioning and refrigeration requirement worldwide [4].

Solar energy stands out as the most abundant and sustainable among renewable energy sources [5, 6] Concentrating solar technology (CST) is becoming increasingly popular due to its built-in storage capabilities and numerous socioeconomic advantages. Within the realm of CSTs, the parabolic

Received 7 November 2023; revised 3 May 2024; accepted 28 May 2024

trough collector (PTC) is the most prevalent in the commercial sector, particularly for power generation, process cooling, and heating applications [7]. The concentrated solar power system total capacity is approximately 6275 MW worldwide [8] and of which 77% of participation is just from PTC [9]. In this sense, CST is a clean and renewable type of energy capable of supplying the world's energy demand in its various applications. In addition, in conditions of higher temperature, these technologies are more appropriate. The PTC is the most developed concentrating system suitable for temperature ranges between 150°C and 400°C [10]

PTCs can be categorized according to their type of absorption: indirect absorption PTC (IDAPTCs) and direct absorption PTC (DAPTCs). IDAPTCs have some major challenges, which include increased thermal loss, low efficiency, and the selected coating instabilities, specifically in conditions with high temperatures [11, 12]. In contrast, DAPTCs directly absorb solar radiation via the heat transfer fluid (HTF), which reduces thermal loss and consequently improves efficiency. Among HTFs, nanofluids have the applicability in several thermal engineering systems, namely heat exchanger, solar collectors, fuel cells, etc. [13]. Studies show that nanoparticles have considerable thermal conductivity [14].

Research has examined various factors such as HTF, geometric dimensions, and operating conditions. Padilla *et al.* [15] conducted an exergy analysis on IDAPTC. Their results indicated that the primary source of exergy destruction was the heat transfer from the sun to the absorber tube, while optical losses significantly contributed to exergy losses. On the other hand, a study by Allouhi *et al.* [16] evaluated the impact of various nanoparticles on Intensity Non-uniformity Distribution Photothermal Conversion (INDPTC) for applications of high and medium temperatures. The maximum efficiency was achieved by CuO nanoparticles, which was in the order of 9.05%.

Moreover, numerous analytical and experimental investigations have been conducted on direct absorption collectors. Liang *et al.* [17] proposed a model of a direct absorption PTC. It was reported that direct absorption collector outperforms the indirect absorption collector. In addition, it was pointed out that enhancement of the glass emittance and transmittance remarkably increments the performance of the system. Menbari *et al.* [17] studied the effect of a CuO/water nanofluid and a binary nanofluid on the DAPTC [18]. The effects of volumetric nanofluid concentration and mass flow rate on thermal efficiency were also analyzed. Heyhat *et al.* [19] examined how the use of nanofluids, metal porosomes, and their combination influenced the performance of DAPTCs. In general, there is a lot of research related to this topic. On the other hand, and in the studies carried out on absorption refrigeration, some of the following are mentioned: Vasilescu and Infante Ferreira [20] studied the LiNO 3 absorption chiller together with parabolic trough solar collectors (PTC) in a Mediterranean climate. The reported results show that a 1000-m^2 area of PTCs is adequate to satisfy more than 50% of the cooling demands required for a slaughterhouse with a maximum cooling load of 600 kW under the climatic conditions of Nápoles, Italia [21].

Moreover, among the research conducted in recent years on the use of solar technologies to drive cooling systems for classrooms, residential sector, buildings, and the industrial sector, below are some of these studies:

Narayanan *et al.* [22] studied solar cooling systems for residential applications for Australian climatic conditions, using TRNSYS software, given the few investigations that have been developed for this country. With the objective of determining the technical, economic, and environmental feasibility of the operation of an evacuated tube collector (ETC), the system, which includes a hot water storage tank and an absorption chiller, was analyzed focusing on the power consumption and performance of its components. The study found that a collector area of 20 m^2 with a storage ratio of 0.02 m^3/m^2 yields a high solar fraction (SF) of 0.91, maintaining temperatures between 20°C and 24°C. This configuration resulted in cost savings of 1477 USD compared to a vapor compression chiller system, with a payback period (PP) of 15.38 years. The cost of the solar refrigeration system was 58 000 USD, compared to the reference cost of the vapor compression system at 73500 USD. Additionally, the solar system achieved emissions savings of 0.003 tons of CH_4, 0.001 tons of N_2O, and 2 tons of CO_2 relative to the chiller system.

Noferesti *et al.* [23] developed in their research simulations with TRNSYS software an analysis for the integration of solar collector systems to heat absorption cooling systems, with the aim of analyzing the reductions achieved in relation to air quality and reduction in energy consumption in buildings in the city of Chabahar, Iran. Three types of solar collectors were simulated in this study: evacuated tube, glazed, and unglazed solar collectors were studied. The findings indicate that for standard office building hours, the cooling system using these collectors improved indoor temperatures by up to 3.08°C, 1.68°C, and 1.46°C, respectively. This led to energy consumption reductions of up to 84%, 64%, and 48%, respectively, compared to the existing cooling system in the building. For all three configurations, the coefficient of performance (COP) value of the absorption cooling system increased from 0.72 to 2.5, 2.28, and 1.96, respectively.

Hadi Alaskaree [24] investigated on the use of solar-powered absorption cooling systems coupled to a hot water storage tank for summer weather conditions in the city of Baghdad, Iraq. In this study, flat plate collectors connected to an absorption cooling system using a lithium bromide-water working fluid were utilized to meet the cooling needs of a 50-m^2 classroom at Baghdad University of Technology. The findings indicate that a tank capacity of 50 kg/m^2 of solar collector area is required to satisfy the cooling load post-energy harvesting period. Additionally, the study demonstrated the benefits of thermal insulation systems, showing that insulation in walls and ceilings can reduce cooling loads. The maximum cooling load reached 9.4 kW in July, roughly equivalent to 30 m^2/ton, attributed to effective thermal insulation. Without insulation, the cooling system could cover only 20 m^2 of the classroom area specified in the study.

Kumar *et al.* [25] developed a thermo-economic optimization analysis of the performance of a single-effect absorption refrigeration system coupled to a solar collector system and a sensitive storage system, a system used for cooling milk plant located in Jaipur (India). In this study, the response surface methodology is used to model a real vapor compression refrigeration system from measurement data of the operation of this type of system. Meteorological data from 2022 were used in the performance and productivity analysis of this study. The results show that during most of the summer months, the system can produce the desired cooling to process 1000 L of milk in 3 hours according to ISO 5708-2 II standards. In addition, the cooling system still has enough heat to cool another 1000-L capacity milk cooling tank. During winter days, the system requires a significant response time to reach thermal energy storage up to 95°C; beyond this point, the system's performance drops considerably due to weak solar insolation. It is unable to provide cooling during the first milking session. The system generates up to 2356 kWh of cooling energy per month in summer, which decreases to 620 kWh during the monsoon and winter seasons. The maximum coefficient of performance achieved is 0.55, with an average of 0.41 to 0.46 during summer months, and 0.34 to 0.39 during monsoon and winter days. The energy efficiency ratio of the system varies between 2.5 and 6.5, with an overall average of 4.55, outperforming conventional vapor compression cooling systems. The levelized cost of energy for the solar-powered absorption cooling system (SPACS) is estimated at $0.177/kWh, with a simple PP of 12.4 years and a discounted PP of 19.7 years.

Gündüz Altiokka and Arslan [26] in their research implemented a methodology for the design and optimization of heat absorption systems for residential applications, with an area of 120 m^2, under conditions of low solar irradiation. Four types of solar collectors were simulated, such as flat plate (FPC), evacuated tube (ETC), compound parabolic (CPC), and parabolic trough (PTC). The absorption system consists of two thermal storage units to guarantee a full day's operation. This equipment consists of a single stage, and its working fluid is ammonia–water (NH_3–H_2O). Among the main results found in this study, it is highlighted that the configuration with ETCs resulted in the most profitable system, with a net present value of 6726.13 USD. While the configuration with PTCs was the most efficient with the highest exergy efficiency (3.38%) and COP value (0.32) among the different configurations evaluated. This research was able to determine that the initial investment of the solar absorption refrigeration system was 7698.75 USD, compared to an initial investment of 10249.06 USD for a conventional vapor compression refrigeration system. Additionally, it was determined that, with the operation of the solar system, energy savings of 533.25 kWh/year and a reduction in CO_2 emissions of 3546.06 kg/year would be achieved.

Mehmood *et al.* [27] in their studies conducted an analysis of an absorption chiller system, driven, coupled to a latent heat storage system, driven by solar energy, using ETCs, for extreme heat weather conditions. The absorption chiller has a cooling capacity of 17.6 kW and handles a mixture of lithium bromide and water as the working fluid. In this research, TRNSYS software was used to develop a parametric study to determine an optimal configuration and its most critical parameters, such as the size of the solar field, the volume of the energy storage tank, the thermal insulation of the tank, the set point of the auxiliary heating system, and the tilt angle of the solar collectors. This configuration was evaluated against an absorption cooling system with a sensible heat storage system (hot water tank) and a vapor compression cooling system. The study found that the latent heat storage system [using phase change materials (PCM)] increased the SF by 4.2% (from 70.3% to 74.5%) due to better temperature stability and 44% lower tank losses. Additionally, although the initial investment cost for the PCM-based solar cooling system is higher than that of the vapor compression system, the life cycle cost is significantly lower in extremely hot climates. Over a 25-year period, the life cycle cost decreased by 34% compared to vapor compression systems and by 9% compared to conventional solar cooling systems. The proposed system also demonstrated a 31.6% savings in primary energy and an annual reduction of 1222 kg CO_2eq in emissions compared to vapor compression cooling technology.

Hakemzadeh *et al.* [28] investigated the technical and economic feasibility of using different types of solar collectors integrated to a heat absorption refrigeration system for tropical climate conditions, such as Malaysia. In this research, it was determined that the ETCs presented the best efficiency to supply heat to the cooling system; in contrast, the linear solar collector systems Frenes and parabolic trough showed high operational efficiencies, mainly for days with little cloud cover. In Ref. [27], the configuration of a photovoltaic-thermal collector system was evaluated, which shows great energy savings and techno-economic potential. For the development of this research, the authors made use of TRNSYS, MATLAB, and REFPROP. The applied analysis was developed to different Mediterranean climatic conditions, and the obtained results reveal that primary energy savings of more than 80% were achieved in all the locations considered [29–33].

As the literature review shows, so far there has been some research on the operation of cooling systems powered by solar energy. However, in these studies, they are limited to evaluate the operation of the solar field system, for fluids usually used in commercial plants, without evaluating in depth the benefits of nanofluids in the operation of real systems, operating in medium temperature range (up to 115°C). In this study to make a first scientific contribution, in relation to the evaluation of the performance of solar concentrating systems, operating with different water-based nanofluids, for an application of a cooling system that is currently in operation at the Universidad Tecnológica de Bolivar (UTB), in Cartagena Colombia. A second scientific contribution, and based on the review of the literature, not shown in other studies is the calculation of positive effect or mitigation of pollutants, obtained when a system such as the absorption refrigeration system installed at UTB, which operates with the burning of natural gas, is replaced by a thermal source such as the parabolic trough system proposed in this research study.

This study presented, it is important to highlight the impact that are having research on the integration of renewable technologies such as solar collectors to the operation of cooling systems by heat absorption. This type of study, energy performance is evaluated, and the environmental and economic impact that has the implementation of this type of system. The authors of this research evaluate the performance of this type of systems for low and high eradication conditions, as well as for tropical climates, for applications in office buildings, classrooms, and the residential sector, mainly. In the case of the simulated technologies, the analysis of flat plate (FPC), evacuated tube (ETC), linear Fresnel (LFC), compound parabolic (CPC), and parabolic trough (PTC) systems is highlighted for the solar field. For this type of technologies, the authors of the different studies highlight the economic viability generated using ETCs, with a lower performance of the system in general, while it is emphasized that when using PTCs, a higher efficiency is obtained, obtaining an increase in the investment due to the cost of the solar field. In the case of the cooling system, the versatility of the heat absorption systems to operate in an integrated way with different types of solar collectors stands out. In the research presented above, it

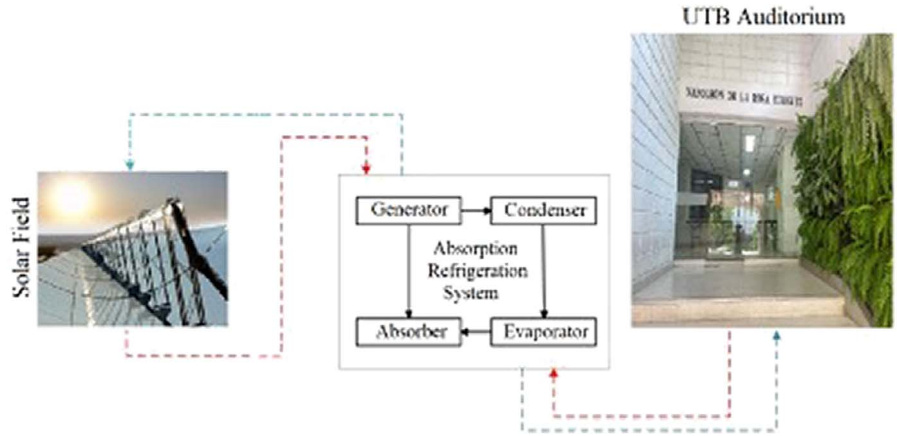

Figure 1. Representation of the proposed system.

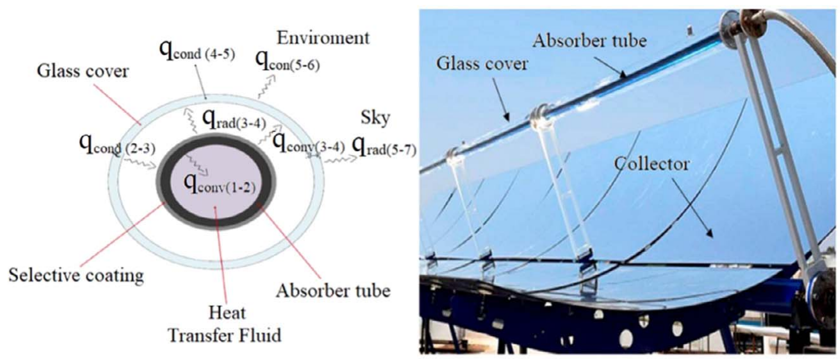

Figure 2. PTC heat transfer model. Adapted from [28–32].

is possible to identify that despite the high cost of cooling systems that represent heat absorption cooling integrated solar collectors, these have a lower cost in relation to conventional vapor compression chiller systems required to supply the thermal load in buildings. In almost all these investigations, the authors chose to use the TRNSYS software to perform the simulations of the different configurations evaluated. Thus, these studies do not include a detailed description of the mathematical models used to characterize the technologies for solar cooling system configurations.

On the other hand, as contributions of our study, we implemented the system configuration using parabolic trough solar collectors and absorption solar cooling system. This configuration is the one with the best performance, according to the authors of the different publications already mentioned. In the case of the solar field, the use of different types of HTFs was evaluated to analyze their performance at different operating temperatures, and the influence of opto-geometric parameters on the performance of the solar collectors integrated to the heat absorption cooling system was also evaluated. An analysis not observed in any of the investigations presented in the state of the art mentioned earlier, which are often limited to the analyses and conditions permitted by the TRNSYS software.

2 Methodology

Fig. 1 shows the scheme of the system proposed in this research study in order to meet the cooling load (369.3 kW) installed in the Napoleon de Rosa Echavez auditorium of the UTB, located in Cartagena Colombia, using PTC technologies.

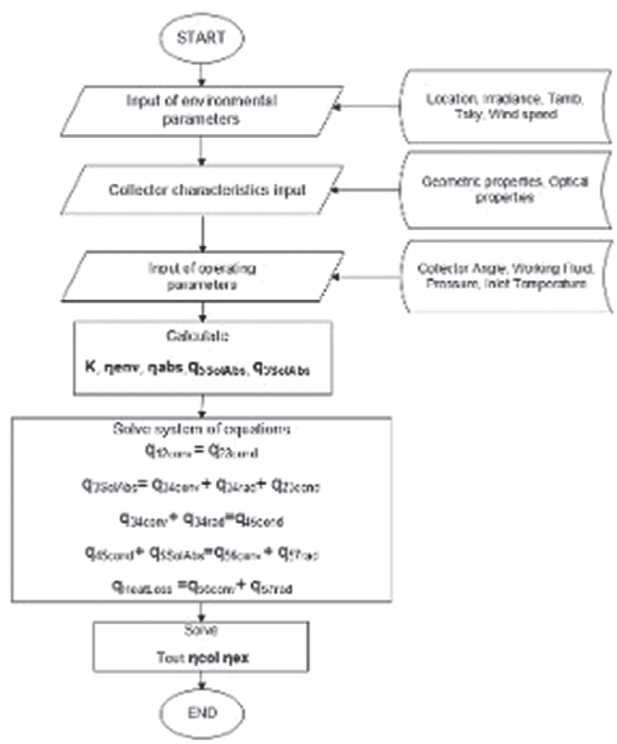

Figure 3. PTC system calculation methodology.

For the absorption refrigeration system (AR) at the Bolivar Technological University, which currently operates by burning natural gas to supply thermal energy, this study proposes

Table 1. Principal equations to characterize the PTC system

System section	Equation		Reference
Glass cover	$\dot{q}'_{5SolAbs} = \dot{q}'_{si}\eta_{env}\alpha_{env}$	(3)	[26]
Absorber tube	$\dot{q}'_{3SolAbs} = \dot{q}'_{si}\eta_{abs}\alpha_{abs}$	(4)	[33]
Inside of the absorber tube	$\dot{q}'_{conv(1-2)} = h_1 D_2 \pi \left(T_2 - T_1\right)$	(5)	[34]
Absorber tube wall	$\dot{q}'_{cond(2-3)} = \frac{2\pi K_{2-3}(T_2 - T_3)}{lnln\left(\frac{D_3}{D_2}\right)}$	(6)	[35]
Absorber outer surface – vacuum condition	$\dot{q}'_{conv(3-4)} = h_{3-4} D_3 \pi \left(T_3 - T_4\right)$	(7)	[36]
	$h_{3-4} = \frac{k_{std}}{\frac{D_3}{2lnln\left(\frac{D_4}{D_3}\right)} + b\lambda\left(\frac{D_3}{D_4} + 1\right)}$	(8)	
	$b = \frac{(2-a)(9\gamma - 5)}{2a(\gamma + 1)}$	(9)	
	$\lambda = 2.331E\left(-20\right)\frac{T_{3-4} + 273.15}{Pa\delta^2}$	(10)	
Absorber outer surface – annular space pressure	$\dot{q}'_{conv(3-4)} = \frac{2.425 k_{3-4}(T_3 - T_4)\left(\frac{PrPr\ R\ a_{D3}}{0.861+}\right)^{\frac{1}{4}}}{\left(1 + \left(\frac{D_3}{D_4}\right)^{\frac{3}{5}}\right)^{\frac{5}{4}}}$	(11)	[32]
Absorber outer surface	$\dot{q}'_{rad(3-4)} = \frac{\sigma\pi D_3\left({T_3}^4 - {T_4}^4\right)}{\frac{1}{\varepsilon_3} + \frac{(1-\varepsilon_3)D_3}{\varepsilon_4 D_4}}$	(14)	[37]
Glass coating	$\dot{q}'_{cond(4-5)} = \frac{2\pi K_{4-5}(T_4 - T_5)}{lnln\left(\frac{D_5}{D_4}\right)}$	(15)	[35]
Outer surface of the glass covering	$\dot{q}'_{conv(5-6)} = h_{5-6} D_5 \pi \left(T_5 - T_6\right)$	(16)	[38]
Outer surface of the glass covering	$\dot{q}'_{rad(5-7)} = \sigma D_5 \pi \varepsilon_5 \left(T_5^4 - T_7^4\right)$	(17)	[39]
Collector	$\eta_{col} = \frac{Q_{Winned}}{I_{irradiance} A_a}$	(18)	[40]

replacing fossil fuel with the implementation of a PTC. Below are the main equations needed to characterize the operation of both a PTC system and an AR.

2.1 Analysis of the solar field in the PTC configuration

This section presents the mathematical model implemented in this study, with the objective of characterizing the operation of the solar field. In this way, it is possible to determine operational parameters such as HTF temperature at the output of the solar field, the efficiency of the solar field. Additionally, the performance variation of this technology can be determined in relation to the variation of certain project parameters and the type of HTF used.

In Fig. 2, a simplified scheme of a PTC system is presented. In this figure, the mechanisms through which solar irradiation reaches the HTF in the receiver system are shown, as well as the mechanisms of heat loss in each section of the receiver.

In Fig. 3, the calculation algorithm implemented in this study is shown to characterize the PTC.

Based on the methodology proposed in Fig. 3, the main equations used for the mathematical development of this mathematical model will be presented below. The mathematical model is evaluated for a division of the collector into N equal parts. Furthermore, it is assumed that the heat transfer by the fluid is only in the longitudinal direction. For steady-state conditions, the energy balance is obtained with equation (1) [25]

$$0 = \left(q_{3SolAbs,i} + q_{5SolAbs,i} - q_{rad(5-7),i} - q_{conv(5-6),i}\right)\Delta L_{tube} + mc_p\left(T_{i,in} - T_{i,out}\right) \quad (1)$$

Taking heat loss into account, the outlet temperature of each differential element can be calculated, and in this way, the temperature at the outlet of the collector can be determined using the equation (2):

$$T_{out} = T_1 + \left(\frac{q_{3SolAbs,i} + q_{5SolAbs,i} - q_{rad(5-7),i} - q_{conv(5-6),i}}{mc_{p_{1-2}}}\right)\Delta L_{tube} \quad (2)$$

Table 1 below shows the main mathematical relationships required to solve equation (2).

2.2 Solar field exergy analysis in the PTC configuration

The exergy analysis is of vital importance to determine the thermodynamic quality of the process. In the parabolic trough, the first analysis corresponds to the exergy flux related to the incoming solar radiation (I) and is obtained by equation (19). The temperature of the sun (T_o) is taken with a value of 5770 K [41]

$$\psi_s = A_a I\left[1 + \frac{1}{3}\left(\frac{T_{env}}{T_s}\right)^4 - \frac{4}{3}\frac{T_{env}}{T_s}\right] \quad (19)$$

The exergy transferred to the operating fluid from the receiver or useful exergy can be calculated by equation (20)[42]:

$$\psi_U = mc_p\left[\left(T_{out} - T_{in}\right) - T_{env} lnln\left(\frac{T_{out}}{T_{in}}\right)\right] \quad (20)$$

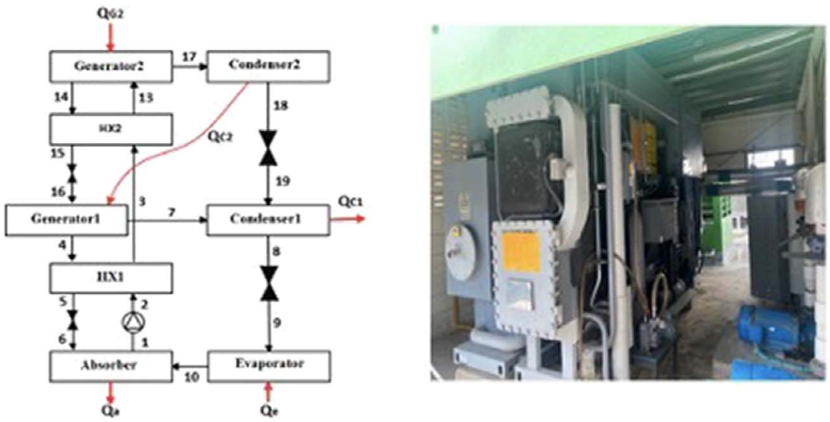

Figure 4. Series double-effect absorption cooling system. (a) Adapted from [32], (b) photo taken from UTB.

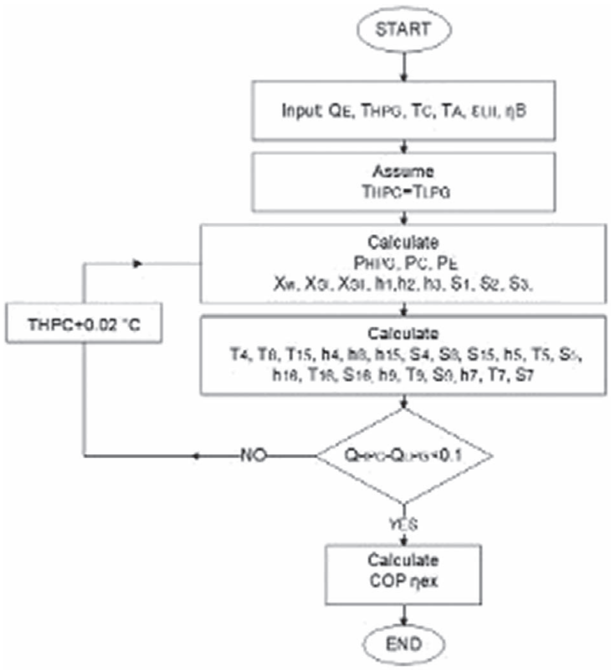

Figure 5. System calculation methodology AR.

We can define the exergy efficiency as the ratio between the input exergy and the useful exergy produced, as expressed in equation (21) [43]:

$$\eta_{\psi} = \frac{\psi_u}{\psi_a} \tag{21}$$

On the other hand, it is possible to calculate the exergy losses related to heat losses. The exergy losses due to optical factors are obtained as expressed in equation (22) [44]:

$$\psi_{losses,opt} = \left(1 - \eta_{opt}\right) \cdot \psi_s \tag{22}$$

Exergy thermal losses are described by the following formulation (23) [44]:

$$\psi_{losses,term} = Q_{losses} \cdot \left(1 - \frac{T_{env}}{T_r}\right) \tag{23}$$

η_{opt} is the optical efficiency, T_r is the temperature in the absorption tube, and Q_{losses} are the heat losses in the collector. Finally, the calculation of the exergy destruction is made up of the exergy destruction between the sun and the absorber and the exergy destroyed between the absorber and the transfer fluid. The value of Q_u corresponds to the heat gained by the collector [44].

$$\psi_{destroyed} = \eta_{opt} \cdot \psi_s - Q_{abs}\left(1 - \frac{T_{amb}}{T_r}\right) + Q_u\left(1 - \frac{T_{amb}}{T_r}\right) - \psi_u \tag{24}$$

2.3 Absorption refrigeration system analysis

In this study, a double-effect absorption refrigeration system with a series configuration (Fig. 4) is going to be studied in order to meet a cooling load of 369.3 kW, UTB Auditorium (shown in Fig. 4), and operate with temperatures below 120°C in the high generator. Under these operating conditions, the double-effect system presents high COP values.

The cycle operates under three pressure levels and consists mainly of two generators, one high temperature (Generator 2) and one low temperature (Generator 1). It also has two condensers, an evaporator, an absorber, two heat exchangers, a solution pump, and four expansion valves. The heat input (Q_{G2}) in Generator 2 is supplied by the solar field, while in Generator 1, the heat is obtained from the high temperature condenser (Condenser 2) [45].

For the analysis of refrigeration systems, the following assumptions are made [46]:

- The cycle is analyzed in steady state.
- There are no heat or pressure losses in the components.
- The outlet of condenser is taken as saturated liquid.
- The outlet of evaporator is taken as saturated vapor.
- The flow through the valves is isentropic.

Fig. 5 shows the calculation methodology implemented to characterize the behavior of absorption refrigeration system studied in this study.

In Fig. 5, sequence of calculations required to characterize the cooling system proposed in this study is shown. In addition to the condition that is necessary to achieve in the calculation algorithm, the iterative process was implemented in the proposed methodology (Fig. 5). Based on this calculation

Table 2. Main equations to characterize the AR, based on the methodology presented in Fig. 5

System section	Equation		Reference
Absorber	$m_1 = m_6 + m_{10}$	(25)	[47–49]
	$m_1 x_1 = m_6 x_6 + m_{10} x_{10}$	(26)	
	$Q_a = m_6 h_6 + m_{10} h_{10} - m_1 h_1$	(27)	
	$m_6 \psi_6 + m_{10} \psi_{10} = m_1 \psi_1 + Q_a \left(1 - \frac{T_o}{T_{abs}}\right) + \psi_{destroyed\_abs}$	(28)	
Generators	$m_{13} = m_{14} + m_{17}$	(29)	[50, 51]
	$m_{13} x_{13} = m_{14} x_{14} + m_{17} x_{17}$	(30)	
	$m_{16} = m_4 + m_7$	(31)	
	$m_{16} x_{16} = m_4 x_4 + m_7 x_7$	(32)	
	$Q_{G2} = m_{14} h_{14} + m_{17} h_{17} - m_{13} h_{13}$	(33)	
	$Q_{c2} = m_7 h_7 + m_4 h_4 - m_{16} h_{16}$	(34)	
	$m_{13} \psi_{13} = m_{14} \psi_{14} + m_{17} \psi_{17} + \psi_{destruida}$	(35)	
	$m_{16} \psi_{16} = m_4 \psi_4 + m_7 \psi_7 + \psi_{destruida\_G1}$	(36)	
Condensers	$m_{17} = m_{18}$	(37)	[51, 53, 54]
	$m_{17} x_{17} = m_{18} x_{18}$	(38)	
	$m_8 = m_7 + m_{19}$	(39)	
	$m_8 x_8 = m_7 x_7 + m_{19} x_{19}$	(40)	
	$Q_{C2} = m_{17} \left(h_{17} - h_{18}\right)$	(41)	
	$Q_{C1} = m_7 h_7 + m_{19} h_{19} - m_8 h_8$	(42)	
	$m_{17} \psi_{17} = m_{18} \psi_{18} + \psi_{destruida\_C2}$	(43)	
	$m_7 \psi_7 + m_{19} \psi_{19} = m_8 \psi_8 + Q_{C1} \left(1 - \frac{T_o}{T_{Cond1}}\right) + \psi_{destroyed\_C1}$	(44)	
Evaporator	$m_9 = m_{10}$	(45)	[48–53]
	$Q_E = m_{10} \left(h_{10} - h_9\right)$	(46)	
	$m_9 \psi_9 + Q_E \left(1 - \frac{T_o}{T_{evap}}\right) = m_{10} \psi_{10} + + \psi_{destruida\_evap}$	(47)	
Heat exchangers	$m_2 \left(h_3 - h_2\right) = m_4 \left(h_4 - h_5\right)$	(48)	[50–53]
	$\varepsilon_{Hx1} = \frac{T_3 - T_2}{T_4 - T_2} = \frac{T_4 - T_3}{T_5 - T_3}$	(49)	
	$m_3 \left(h_{13} - h_3\right) = m_{14} \left(h_{14} - h_{15}\right)$	(50)	
	$\varepsilon_{Hx2} = \frac{T_{13} - T_3}{T_{14} - T_3} = \frac{T_{14} - T_{13}}{T_{15} - T_{13}}$	(51)	
	$m_2 \psi_2 + m_4 \psi_4 = m_3 \psi_3 + m_5 \psi_5 + \psi_{destruida\_HX1}$	(52)	
	$m_{14} \psi_{14} + m_3 \psi_3 = m_{13} \psi_{13} + m_{15} \psi_{15} + \psi_{destroyed\_HX2}$	(53)	
Valves and pump	$h_5 = h_6$	(54)	[50–53]
	$h_8 = h_9$	(55)	
	$h_{15} = h_{16}$	(56)	
	$h_{18} = h_{19}$	(57)	
	$m_1 h_1 + w_{B1} = m_2 h_2$	(58)	
	$w_B = \frac{m_1 (P_2 - P_1)}{\rho \eta_B}$	(59)	
	$m_1 \psi_1 + W_B = m_2 \psi_2 + \psi_{destruida\_B}$	(60)	
Efficiencies cooling systems	$COP = \frac{Q_E}{Q_{G2} + W_{B1}}$	(61)	[48–53]
	$ECOP = \frac{Q_E \left(1 - \frac{T_O}{T_{Evap}}\right)}{Q_{G2} \left(1 - \frac{T_O}{T_{Gen2}}\right) + W_{B1}}$	(62)	

Table 3. Emission factors for each agent emitted from natural gas Adapted from [56].

Energy source	Agent issued	Emission factor	
		As a function of thermal input power (lb/MMBtu)	As a function of thermal input power (kg /kW h)
Natural gas	Nox	3.20E−01	4.95E−04
	CO	8.20E−02	1.27E−04
	CO_2	110	1.70E−01
	N_2O	0.003	4.64E−06
	SO_2	0.94	1.45E−03
	Metano	8.60E−03	1.33E−05
	VOC	2.10E−03	3.25E−06
	TOC	1.10E−02	1.70E−05
	PM (condensable)	4.70E−03	7.27E−06
	PM (filtrable)	1.90E−03	2.94E−06
	PM (total)	6.60E−03	1.02E−05

Table 4. Initial parameters of PTC

Parameters	Value	Parameters	Value
Tamb (°C)	21.2	Absorber tube external diameter (m)	21.2
Vwind (m/s)	2	Absorber tube inner diameter (m)	0.066
Aperture W (m)	5	Covered transmittance	0.95
Length (m)	7.8	Surface reflectivity	0.93
Outer casing diameter (m)	0.115	Coated absorptivity	0.906
Cover inner diameter (m)	0.109	Coated Conductivity (W/mK)	1.2
Absorber conductivity (W/mK)		54	

Table 5. Validation of the PTC model

				Model [59, 60]	Model UTB		Model [61]	Model UTB	
Fluid	$\dot{m}$ (kg/s)	Ib (W/m^2)	Tin (°C)	Tout-Tin (°C)		Difference (%)	η (%)		Difference (%)
Therminol VP1	0.6782	933.7	102.2	22.3	22.1	0.9	–	–	–
Therminol VP1	0.6536	937.9	151	22.86	22.2	2.89	–	–	–
Syltherm 800	0.8362	813.1	101.2	17.8	17.8	0.00	71.56	71	0.78
Syltherm 800	0.8794	858.4	154.3	17.4	17.8	2.30	69.2	70.24	1.50

algorithm, the main equations required in this mathematical model will be presented below.

Table 2 shows the equations used to develop the thermal, exergy, species flow ratio and heat flow analysis of the different components of the AR.

In the Fig. 5 the equations to characterize the AR are shown.

2.4 Analysis of pollutant emissions reduction

This section presents the mathematical relationships required to determine the environmental impact of replacing conventional sources with solar collectors to operate the cooling system. For the comparative analysis, a boiler in which natural gas is burned is considered as a conventional source.

According to the US Environmental Protection Agency (EPA), the following is a list of the most important environmental protection agencies in the United States [55, 56]

$$E = FE_{ij} \cdot FA_{jt} \tag{63}$$

Table 3 shows the emission factor for each of the agents emitted by natural gas during the combustion process.

2.5 Mathematical validation of system models PTC and AR

It is important to note that the double-effect absorption refrigeration system installed in the UTB Auditorium lacks a technical manual, model reference, or instrumentation/meters to maintain historical records of its operational parameters. Before carrying out this research study, we consulted with the different departments of the University, but unfortunately, the University lacks information about the equipment. Given this limitation, the validation of the mathematical model developed in this scientific study was carried out by comparing it with other scientific studies, which do have the necessary operational parameters for validation.

The mathematical model of the PTC is compared with the article presented by Marif *et al.* [57] and García-Valladares and Velázquez [58]. An LS-2 type collector and the environmental conditions are defined as input parameters (Table 4).

The findings are verified in terms of the outlet temperature and the efficiency of the collector. The maximum difference of 2.89% found in Table 5 allows to guarantee that the results obtained by the model presented in this study are quite correct.

Table 6. Double acting AR operating parameters

Component	Parameter	Operating value
HPG	THPG (°C)	130
LPG	TLPG (°C)	80
Capacitor	TC (°C)	35
Absorber	TA (°C)	35
Evaporator	TE (°C)	4
Pump	η_B (%)	95
SHE I, SHE II	$\varepsilon_{I,II}$ (%)	70

2.6 AR double effect

For the evaluation of the double-effect cooling system, the parameters described in Table 6 are defined. The results are compared with the studies of Yilmaz *et al.* [61] and Garousi Farshi *et al.* [62]. At this stage, the operating data from the UTB system were not used due to the lack of instrumentation in the system and damage to some of the system's sensors.

In the validation of the model of the present study, the lithium bromide concentration and enthalpy values of each state are verified. In the comparison presented in Table 7, it is evident that the model used allows obtaining values with a high accuracy (maximum difference of 0.09%).

2.7 Economic study of the system

Another important aspect evaluated in this study is the analysis of the levelized cost of heat (LCOH); this indicator is frequently used to assess the economic performance of thermal systems. The economic analysis will be further enhanced by evaluating the capital cost and annual cash flow.

Table 7. Validation of double-effect AR model

Condition	Substance	T (°C) UTB applied case	T (°C) [63]	X (%) UTB applied case	X (%) [64]	Difference (%)	h (kJ/kg) UTB applied case	h (kJ/kg) [64]	Difference (%)
1	Water	35	35				146.59	146.59	0.00%
2	Water	4	4				146.59	146.59	0.00%
3	Vapor	4	4				2507.87	2507.87	0.00%
4	Weak LiBr	35	35	55.87	55.827	0.08%	87.59	87.67	0.09%
5	Weak LiBr	35	35.02	55.87	55.827	0.08%	87.59	87.67	0.09%
6	Weak LiBr	62.49	62.37	55.87	55.827	0.08%	143.11	143.14	0.02%
7	Weak LiBr	106.8	106.49	55.87	55.827	0.08%	235.54	235.43	0.05%
8	Strong I LiBr	130	130	58.06	58.060	0.00%	288.56	288.40	0.06%
9	Strong I LiBr	83.11	82.69	58.06	58.060	0.00%	192.51	192.49	0.01%
10	Strong I LiBr	83.11	82.69	58.06	58.060	0.00%	192.51	192.49	0.01%
11	Vapor	130	130				2740.54	2740.53	0.00%
12	Water	82.46	82.54				345.25	345.21	0.01%
13	Water	35	35				345.25	345.21	0.01%
14	Vapor	80	80				2649.57	2649.57	0.00%
15	Strong II LiBr	80	80	60.28	60.311	0.05%	195.8	195.84	0.02%
16	Strong II LiBr	48.67	48.52	60.28	60.311	0.05%	135.9	135.98	0.06%
17	Strong II LiBr	48.67	48.52	60.28	60.311	0.05%	135.9	135.98	0.06%

2.8 Levelized cost of heat

This metric enables the comparison of various thermal energy systems, encompassing both renewable and fossil alternatives. The LCOH indicates the cost per unit of energy generated or conserved by the system throughout the project's lifetime. In this study, it was considered that there are no incentives or subsidies. ($S_0 = 0$), no residual value ($RV = 0$), depreciation of assets (DEP_T), and the corporate income tax rate (TR) are equal to zero [65, 66]

Considering these factors, the LCOH can be calculated using the following equation (65) [45].

$$LCO_h = \frac{I_0 + \sum_{t=1}^{L} \frac{C_{O,M_T}}{(1+r)^T}}{\sum_{T=1}^{L} \frac{Q_{U_T}}{(1+r)^T}} \tag{64}$$

where I_0 is the initial investment, $C_{O,MT}$ are operating and maintenance costs (in the year), r is the discount rate, L is the useful life of the power system in years, and Q_{U_T} is the useful energy delivered by the power system to the industrial process in the year t. In this study, C_{O,M_T} are considered to represent the 1% del I_0 [45], T is 25 years old, and r is 10% [68, 67].

The LCOH provides a measure of the average cost of producing a unit of heat over time, allowing comparison of different heat generation technologies. It is a useful tool for assessing the economic viability of heating and cooling systems and can assist in decision-making in energy project planning [67].

2.9 Cost of system capital

The capital cost of the system is evaluated by adding up all the costs of the system components, such as the storage tank, the solar field, and the absorption refrigeration unit [66].

$$C_0 = K_{tank} * V + K_{col} * A_{col} + K_{ch} * Q_e \tag{65}$$

where C_o is the cost of capital in US\$, K_{tank} is the cost of the storage tank in US\$ m^{-3}, V is the storage tank volume in m^3, K_{col} is the cost of the solar collector in US\$ m^{-2}, A_{col} is the collector surface area in m^2, K_{ch} is the cost of the absorption chiller in US\$ $KW_{\text{cool}}{}^{-1}$, and Q_E is the cooling capacity. It should be noted that the configuration of our system did not consider including the presence of a heat storage tank for the process.

The annual cash flow of the system is evaluated as follows [66]:

$$CF = K_{ref} * E_{ref} - (O\&M) \tag{66}$$

where (CF) is the cash flow in US\$, E_{ref} is the annual production of refrigeration in KWh, and $K_{ref}$is the cost of refrigeration US\$calculated according to the methodology of Ref. [44], and ($O\&M$) is the annual cost of operation and maintenance and is valued at the 1% of the cost of capital according to [47].

The cost of refrigeration is evaluated as follows [66].

$$K_{ref} = \frac{K_{el}}{CO\ P_{eq}} \tag{67}$$

where (K_{el}) is the cost of electricity and $\left(CO\ P_{eq}\right)$ is equivalent to the COP of conventional mechanical compression aircondi tioning. Currently, the cost of electricity (K_{el}) is approximately 0.3 US\$/kWh on the Caribbean Coast [67–69].

The equivalent project life is given as follows [47]:

$$R = \frac{(1+r)^N - 1}{r(1+r)^N} \tag{68}$$

where r is the discount factor and N is the useful life of the investment in the present investigation; the discount factor (r) is 10% and the investment lifetime (N) is 25 years.

The net present value of investment is given as follows [70]:

$$NPV = -C_O + R * CF \tag{69}$$

Table 8. Economic analysis parameters

Parameter	Symbol	Value
Solar collector cost per area	K_{col}	298.92 US\$ m^{-2}
Chiller cost per refrigeration power	K_{ch}	656.96 US\$ m^{-2}
Investment lifetime	(N)	25 years
Equivalent lifetime	R	9 years
Cost for operation and maintenance	$O\&M$	$1\% * C_0$

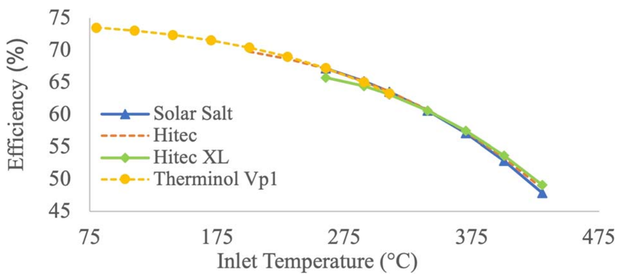

Figure 6. Thermal efficiency of the PTC for different fluids.

Table 9. Main dimensions of the LS-2 PTC

Absorber length (L)	5 m
Width of collector (W)	7.8 m
Absorption pipe outside diameter (D3)	0.070 m
Inner diameter of absorber pipe (D2)	0.066 m
Outer diameter glass liner (D5)	0.115 m
Inner diameter of glass lining (D4)	0.109 m
Shading error	0.974
Tracking error	0.994
Geometric error	0.98
Material gloss error	0.935
Error	0.9675
Unaccounted errors	0.96
Reflectivity	0.935
Emissivities of the exterior glass envelope	0.86
Angle of incidence	0°

The simple amortization period of the investment is determined by equation (46) as follows:

$$SPP = \frac{C_o}{CF} \tag{70}$$

In Table 8, the input parameters of the economic analysis are summarized.

The investment Payback Period (PP) considers the change in the value of money over time. Assuming a discount factor (r), can be determined with the equation [66].

$$PP = \frac{\ln \frac{CF}{CF - C_0 * r}}{\ln\ (1 + r)} \tag{71}$$

At this point, it must be commented that the cash flow of the investment CF shows the yearly net benefits, and it considers the profit by selling the refrigeration and the maintenance and operation costs.

3 Results and discussion

3.1 Results of the analysis of the operation of AR systems coupled to the PTC system

This section presents the main results of the operation of the cooling system coupled to the solar concentrator system. Initially, an analysis of the PTC system operating with different HTFs is presented. From this analysis, the most adequate configuration of the solar field, to be integrated to the cooling system, is determined to satisfy the thermal load of the UTB Auditorium.

In the study, the main characteristics of a PTC LS-2 have been selected. The fixed input parameters such as width, length, diameters, and efficiencies of some elements are presented in Table 9.

Fig. 6 shows the thermal efficiency performance of the PTC system, evaluated for the parameters shown in Table 6.

Fig. 6 shows the efficiency comparison between the different salts and Therminol VP1, which is one of the most

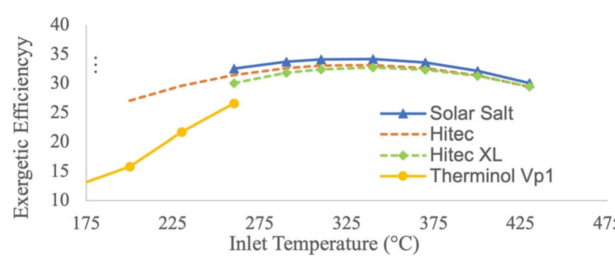

Figure 7. Outlet temperature of the parabolic trough for different fluids.

commonly used fluids in this type of collectors. As can be seen in the figure, for temperatures below 200°C, Therminol VP1 allows obtaining higher efficiencies for this type of technology, in relation to the other fluids used. For temperatures from 75°C to 300°C, Therminol VP1 achieves better energy efficiency values for the solar field, followed by Hitec salt. It is important to note that the efficiency of Hitec XL for inlet temperatures above 325°C manages to exceed the energy efficiency of the other two thermal salts.

Fig. 7 shows the energy performance of the PTC system, operating with different HTFs evaluated in the proposed system.

For the different salts used in the analysis, higher energy efficiency values are obtained than those obtained with Therminol VP1 (Fig. 7). The highest efficiency is achieved for the system configuration working with solar salt, followed by the configuration working with Hitec, Hitec XL, and Therminol VP-1. For the conditions evaluated in the solar field, higher exergy efficiencies were achieved for operating temperatures close to 335°C. For the analysis of the use of nanofluids in the energetic and exergetic performance of collectors, this study describes the behavior of HTFs such as water, with the use of

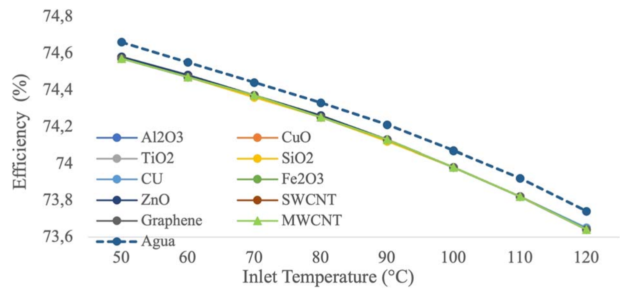

Figure 8. Efficiency of the PTC for water-based nanofluids.

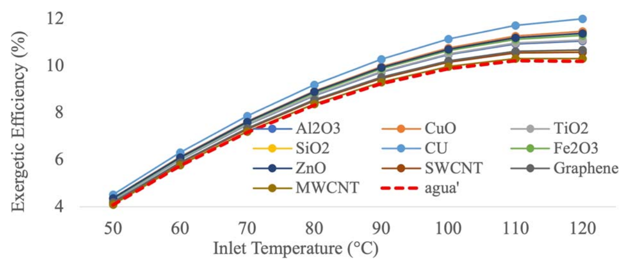

Figure 9. Exergetic efficiency of a PTC for water-based nanofluids.

Al_2O_3, CuO, TiO_2, SiO_2, Cu, Fe_2O_3, ZnO, graphene, Multi-Walled Carbon NanoTubes (MWCNT), and Single-Walled Carbon NanoTube (SWCNT) nanoparticles. In the literature, nanoparticles are evaluated at different concentrations. However, to simplify the calculations and to obtain a preliminary study of the behavior of the nanofluids, the concentrations for all the nanoparticles are 1.5% (Fig. 8).

Fig. 8 shows the thermal efficiency curve of the PTCs. As can be seen for the conditions evaluated, water presents better thermal efficiency values of the solar field than the different nanofluids. In the case of nanofluids, no differences are observed in the thermal efficiency values of the system.

Fig. 9 shows the behavior of the exergy efficiency of the solar field, operating with different HTFs. With water as the reference fluid, the concentration in different particles is 1.5%.

From Fig. 9, for temperatures below 70°C, there is no considerable difference between the exergy efficiency values of the fluids used in the solar field. For temperatures above 70°C, the nanofluids present higher efficiency values than water. At a temperature of 120°C, the fluid with the highest exergy efficiency is $A1_2O_3$, with a value of 12%, while water has the lowest exergy efficiency of the system, with a value of 10.2%. In the temperature range evaluated, from 50°C to 120°C, there is no considerable difference in the value of the exergy efficiency for the rest of the nanofluids evaluated for the collector system.

3.2 Analysis of results absorption refrigeration system

From the results presented above and considering the capacity of the cooling system that is installed in the UTB Auditorium, Napoleón de Rosa Echavez, which has a capacity of 369.3 kW. A configuration of the PTC system was obtained, which manages to satisfy the thermal condition of the proposed refrigeration system. Based on the results shown in Fig. 7 and considering the operating conditions of the UTB cooling system, it was decided to evaluate the operation of the collector system, working with water as HTF, given the small

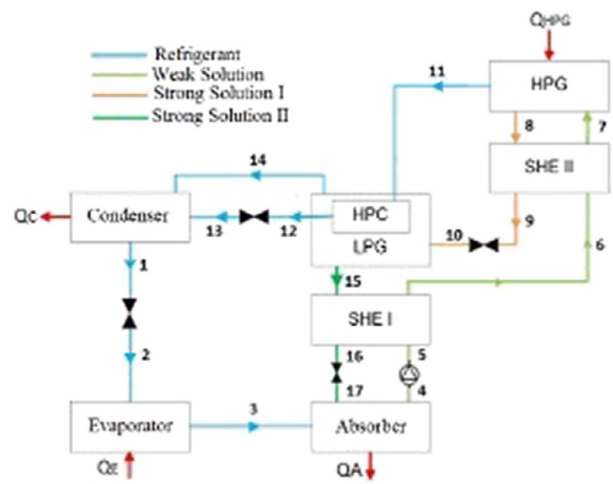

Figure 10. Double-effect series refrigeration system.

difference in the value of the exergy efficiency between the evaluated fluids (Fig. 9). In addition, the configuration of the PTC system is presented, with the nanofluid with the highest exergy efficiency "Al_2O_3" (Fig. 9). In this research, we also chose to present the configuration of the PTC system, working with water, since at moderate operating temperatures, it is economical to work with water, in relation to the higher costs associated with the purchase of Al_2O_3 nanofluids.

Tables 10 and 11 present the optical and geometrical parameters of the solar field that supports the operation of the AR system of the UTB Auditorium, operating with water and with the Al_2O_3 nanofluid, respectively. The ambient conditions used in this analysis are ambient temperature of 28°C, wind speed of 2 m/s, and solar irradiation of 640 W/m^2.

To assess the absorption refrigeration system, a double-effect series configuration (Fig. 10) is chosen to handle a cooling load of 369.3 kW. The findings in this section aim to demonstrate the influence of the operating parameters of the components on the system's energy and energy efficiency. The system uses LiBr–H_2O as the working fluid.

Table 12 shows some of the project parameters defined for the analysis presented in this section.

For the project parameters already defined and shown in Tables 12 and 13, different operating conditions were obtained in the AR system, which are shown in Table 13.

Fig. 11 shows the variation of the COP and LiBr concentration with the change in temperature of the high-pressure generator. The weak (XW) and strong II (XSII) concentration are not affected by the change in Temperature Hight Pressure Generator (THPG) temperature, whereas for the strong I (XSI) solution, there is a decrease at higher temperatures. This is clearly caused by the increase in operating pressure. On the other hand, the COP of the system decreases at higher temperatures.

The effect of the low condenser temperature (CT) on the COP and LiBr concentration is presented in Fig. 12. In this, there is a decrease in the COP with increasing CT. With the increase in CT, the enthalpy of the refrigerant in States 1–2 increases, and therefore, the mass flow also increases, since it has a constant cooling load and the enthalpy of State 3 remains the same; likewise, the mass flow circulating in the high generator increases and with this the heat flow. As Q_{HPG} increases and QE is a fixed parameter, the COP decreases. In

Table 10. PTC solar field configuration

Fluid	Agua	Series configuration	5
Total mass flow (kg/s)	1.6284	Parallel configuration	3
Collector type	LS-2	Aperture area (m^2)	585
Collector length (m)	7.85	Outlet temperature (°C)	112.2
Manifold width (m)	5	Collector efficiency (%)	74.33

Table 11. Solar field configuration PTC

Fluid	Agua + Al_2O_3	Series configuration	3
Total mass flow (kg/s)	1.9195	Parallel configuration	5
Collector type	LS-2	Aperture area (m2)	588.75
Collector length (m)	7.85	Outlet temperature (°C)	112.2
Manifold width (m)	5	Collector efficiency (%)	74.22

Table 12. UTB AR system project parameters

Parameter	Value
CT (°C)	30
Evaporator temperature (°C)	5
Absorber temperature (°C)	30
Temperature high HPG generator (°C)	100
Low LPG generator temperature (°C)	80
Cooling load Qe (kW)	369,3
Pump efficiency (%)	95
Effectiveness of HX1 HX2 exchangers (%)	70
COP	1438
Pmax (kPa)	17,26
Pm (kPa)	4246
Pmin (kPa)	0,8726

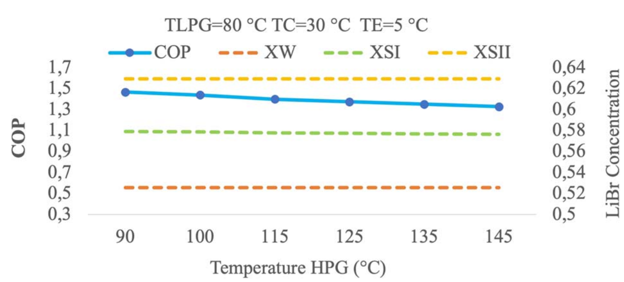

Figure 11. Variation of COP and LiBr concentration with HPG temperature.

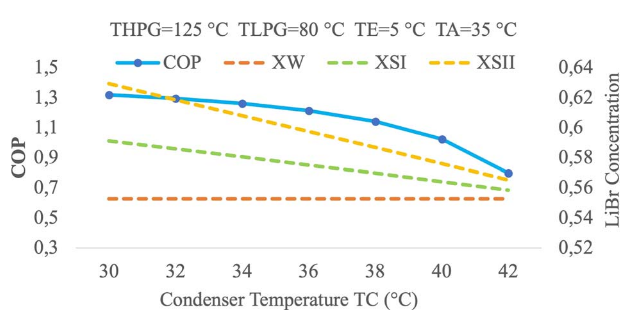

Figure 12. Variation of COP and LiBr concentration with low pressure CT.

relation to the LiBr concentrations, the CT does not affect the weak concentration and the strong concentrations I and II decrease with increasing temperature.

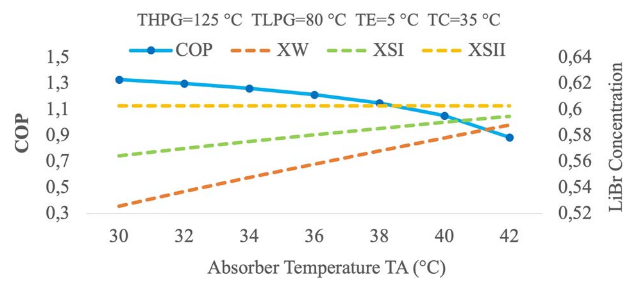

Figure 13. Variation of COP and LiBr concentration with absorber temperature.

In some operating conditions, lowering the temperature in the condenser too much can cause the solution entering the absorber to present crystallization problems. At CTs below 30°C, it is important to check the temperature and LiBr concentration of the solution in States 16 and 17. For high CT values, the difference between the concentrations is reduced and a decrease in the COP of the system is generated.

As in the condenser, increasing the temperature in the absorber generates a decrease in system performance as shown in Fig. 13. Increasing the TA value generates an increase in the mass flow rate of the weak, strong solution line I and, therefore, an increase in Q_{HPG}. The variation of the temperature in the absorber does not generate any change in the concentration of the strong solution II. For weak and strong solution I, the concentration increases with temperature and tends to narrow the difference between them.

For the behavior shown in Fig. 14, the components with the highest exergy destruction are the high generator, the absorber, the evaporator, and the SHE II heat exchanger. With the change of the Temperature Hight Pressure Generator (HPG) temperature, components such as the low condenser, the two generators, and the heat exchanger present variations in the exergy destroyed. It should be noted that the temperature change in the high generator only generates changes in the destroyed exergy of the SHE II heat exchanger, while the other remains constant. In the generator itself, with the increase in temperature, the exergy flow increases, and with it the destroyed exergy of the equipment.

As for the HPG temperature variation, the components with the highest exergy destruction are the evaporator and the absorber (Fig. 15). The variation of exergy destruction for the

Table 13. Operating status and properties of the UTB AR system in the proposed solar configuration

State	T (°C)	P (kPa)	m (kg/s)	h (kJ/kg)	s (kJ/kg-K)	x LiBr
1	30	4.246	0.1549	125.67	0.4365	
2	5	0.8726	0.1549	125.67	0.4525	
3	5	0.8726	0.1549	2509.71	9.024	
4	30	0.8726	0.9406	66.59	0.1943	0.5257
5	30	17.26	0.9406	66.59	0.1943	0.5257
6	55.12	17.26	0.9406	119.44	0.362	0.5257
7	81.74	17.26	0.9406	176.89	0.5295	0.5257
8	100	17.26	0.855	226.11	0.5803	0.5784
9	68.77	17.26	0.855	162.91	0.404	0.5784
10	68.77	4.246	0.855	162.91	0.404	0.5784
11	100	17.26	0.08559	2686.09	8.193	
12	56.92	17.26	0.08559	238.26	0.7923	
13	30	4.246	0.08559	238.26	0.8079	
14	80	4.246	0.06932	2649.78	8.74	
15	80	4.246	0.7857	210.15	0.4346	0.6294
16	45.37	4.246	0.7857	146.88	0.2457	0.6294
17	45.37	0.8726	0.7857	146.88	0.2457	0.6294

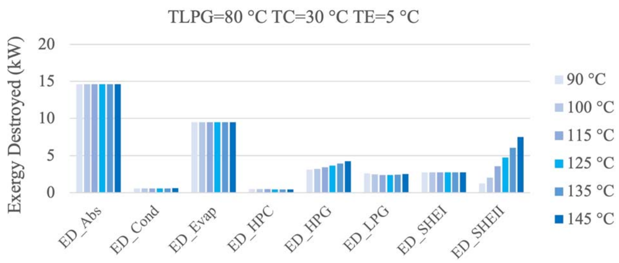

Figure 14. Exergy destroyed with HPG temperature variation.

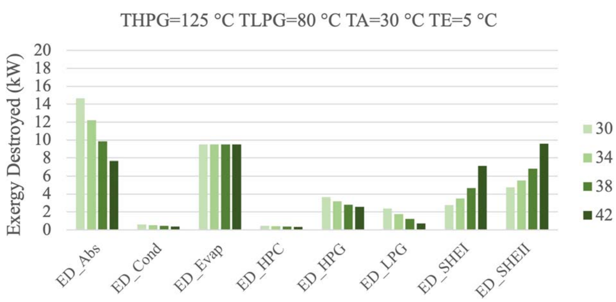

Figure 15. Exergy destroyed with the variation of the CT.

HPG is only 1.1 kW for a change from 30°C to 42°C in the CT. On the other hand, the increase in CT generates a decrease in the exergy flux per mass entering the absorber from the SHEI heat exchanger. This decrease in exergy flux is transformed into less exergy destruction by the absorber.

The change in CT affects the exergy destroyed for the two heat exchangers. In both cases, the increase in CT increases the exergy destruction. For the condenser, the exergy destroyed decreases due to the increase in the outgoing exergy flow by mass and the increase in the exergy leaving due to the heat expelled to the environment.

The change in the exergy destroyed is shown in Fig. 16. With the increase in evaporator temperature, the exergy flow per mass in the evaporator decreases. In addition, it increases the exergy destruction in components such as the absorber and the two generators. For the two exchangers, the exergy destroyed decreases with increasing evaporator temperature.

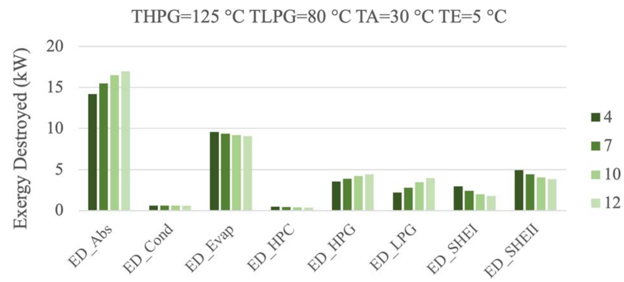

Figure 16. Exergy destroyed with evaporator temperature variation.

3.3 Pollutant emission reduction analysis

In this section, it is important to mention that the UTB cooling system currently operates 100% by means of natural gas combustion. Fig. 17 shows an image of the absorption refrigeration system currently installed at UTB. In the figure, the combustion chamber can be identified, where natural gas is burned during the process.

For the evaluation of emissions, it is assumed that the refrigeration system currently installed at the UTB in Cartagena/Colombia operates with a temperature in the low LPG condenser of 80°C, with a temperature in the condenser–absorber of 30°C and an evaporator temperature of 5°C. The high HPG generator is operated for temperatures from 90°C to 145°C to consider possible variations in heat flow delivered by the natural gas flaring system currently in the UTB system (Fig. 17), heat that will be supplied in this study, by the collector field.

Table 14 shows the different heat flows for the operating condition expressed above.

Fig. 18 shows the emissions of each pollutant generated in the combustion of natural gas for the maximum thermal power input to the AR system (Table 10). As can be seen in the figure, the pollutants with the highest emissions are CO_2, NOx, and SO_2. CO_2 emissions are approximately 50 kg per hour of operation of the refrigeration system.

If the absorption refrigeration system has an operation of 8 hours per day for a year, we can see in Fig. 19, operating with the burning of natural gas, CO_2 emissions exceed 100 tons/year, followed by NOx that can reach 5 tons/year.

Figure 17. UTB Auditorium absorption cooling system.

Table 14. Heat flux delivered to the cooling system with THPG variation

THPG (°C)	COP	QHG (kW)
90	1.466	251.97
100	1.438	256.83
115	1.398	264.09
125	1.373	268.91
135	1.349	273.69
145	1.326	278.45

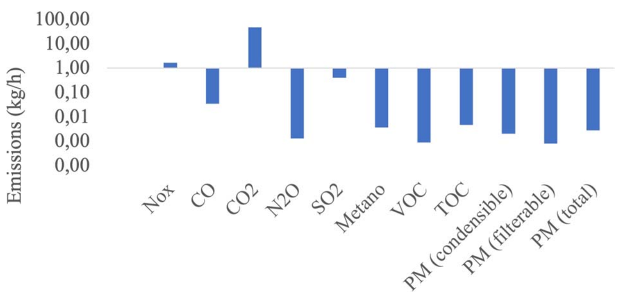

Figure 18. Emissions of natural gas pollutants.

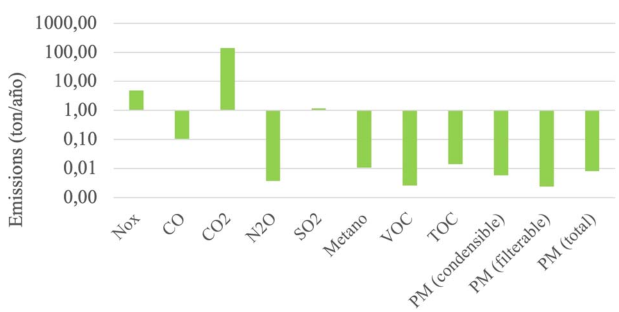

Figure 19. Pollutant emissions by year of operation AR.

3.4 Result of the financial analysis of the system's economic indicators

The results obtained in this analysis are presented in Table 15. They are based on the input parameters defined in the Table 8.

Additionally, it is important to note that from this analysis, it was possible to determine that the equivalent useful life of the project was approximately 9 years, with a PP of 18.9 years. The double-effect heat absorption cooling system, taken as a reference system for this study, is characterized by operating 384 hours/year and is responsible for cooling the auditorium of the Technological University of Bolivar (UTB). It is important to mention that this space is intended for undergraduate and graduate master classes, as well as sociocultural events in the city of Cartagena.

Through this analysis, it was possible to determine the value of the LCOH, which provides an average of the cost of producing one unit of heat over time, which was 213.91 US$ MWh, for the parameters and conditions mentioned above.

4 Conclusions

For the energy analysis of the PTC, thermal efficiencies higher than 70% were found for the conditions evaluated. With respect to the exergetic efficiency of the PTC for temperatures close to 100°C, the collector presented values of 12% in exergetic efficiency; similar results are observed in other studies, such as in Refs. [31, 32, 37].

The results presented in this study show that within the HTFs used commercially in parabolic trough systems, and temperature range above 200°C, the solar salt fluid allows obtaining the highest exergetic efficiencies for the solar field. For operating temperatures up to 120°C (close to the operating temperature of the UTB refrigeration system), the thermal analysis shows that there is no considerable difference in the efficiency value between the water and the water-based nanofluids evaluated in this study. In the research carried out in Ref. [37], similar behaviors are evidenced, in comparison to the results presented in this section of this manuscript. In the case of the exergy analysis, for the temperature range up to 120°C, the nanofluid water + AI2O3 presents the highest exergy efficiency obtained for the solar field configuration. For the fluids evaluated in this analysis, there were no considerable differences in the exergy efficiencies.

In relation to the thermal and exergetic behavior of the simulated double-effect absorption refrigeration system, it was found that the performance decreases with the increase in the temperature of the high generator. The highest COP values are found for low temperatures in the evaporator, absorber, and condenser. With the latter, it is important to verify that the decrease in temperature does not generate crystallization problems in the solution entering the absorber. In the exergy analysis of the system, it was found that the greatest exergy destruction occurred in the absorber, evaporator, and high generator. These results are like those obtained in the investigations [46–49] among other research that could be reviewed, and that these show the potential of this type of system, as a strategy for decarbonization of cooling systems for applications in the residential, industrial, residential, educational, etc. sector.

Table 15. Studied system cost data

Parameter	Symbol	Value
Capital cost C_O	C_O	252.442 US$
Yearly cash flow	CF	30.201 US$
Cost of refrigeration	K_{ref}	0,2 US$ kWhref
Operation and maintenance cost	$O\&M$	2.524,42 US$
Yearly refrigeration production	E_{ref}	1 418 112 kWh
Net present value of investment	NPV	21.696 US$
PP	PP	1 895 997 165 years

It can be concluded that the use of solar collectors to operate absorption refrigeration systems can reduce the emission of pollutants from the combustion of conventional fuels such as natural gas. Thus avoiding the increase of pollutants such as CO_2 and NOx in the atmosphere. In the case study presented in this study, on the refrigeration system of the UTB, it is possible to observe that within the different types of agents emitted by the combustion of natural gas, the main agent produced is CO_2, followed by NOx and SOx. For the conditions defined in this study, it was determined that CO_2 emissions exceeded NOx emissions by 10%, while SOx emissions exceeded SOx emissions by 200%. These results agree with the different conclusions presented throughout the references used in this research, where the authors of these studies highlight the significant contribution of the incorporation of renewable technologies as mechanisms to reduce the carbon emissions generated by the use of different technologies nowadays. As well as the importance of searching for strategies to substitute or generate an integrated operation between these technologies (renewable and conventional), which allow to effectively demonstrate the carbon footprint of the processes.

The economic analysis developed in this research allowed determining some important parameters such as the return on investment, the annual cash flow, and the net present value of the investment, parameters show at Table 15, which compared with some bibliographic references presented in this study, turned out to be similar, some studies such as those published by [22, 25, 26].

As a general conclusion of this research and considering the operating conditions of the cooling system installed at UTB, Cartagena/Colombia, it was identified that it is possible to achieve the operation of the refrigeration system, coupled to a solar field of PTCs, operating with water as HTF, as an economical option to be implemented at the university. Or the incorporation in the previously proposed configuration, of the nanofluid water + AI2O3 as HTF, which would increase the investment costs of the project, but would allow to obtain a better thermal utilization of the energy available in the system.

Acknowledgements

This study proposes to analyze an absorption refrigeration system coupled to a solar collector as an alternative to reduce natural gas consumption and energy and environmental impacts that is tending in the operation of the Technological University of Bolivar (Cartagena-Colombia). Some authors wish to thank the Pilo Paga program for the resources granted to study Mechanical Engineering and the Universidad Tecnológica de Bolívar (UTB) for allowing access to the equipment installed at this University. Some authors also wish to thank the National Agency of Petroleum, Natural Gas and Biofuels (ANP) of Brazil.

Author contributions

Álvaro Arteaga Díaz (Conceptualization [equal], Investigation [equal], Methodology [equal], Writing—original draft [equal]), Gaylord Enrique Carrillo Caballero (Methodology [equal], Validation [equal], Writing—original draft [equal]), Yulineth Cárdenas Escorcia (Validation [equal], Writing—original draft [equal]), Mohammad Hossein Ahmadi (Supervision [equal], Writing—review & editing [equal]), Mohsen Sharifpur (Supervision [equal], Writing—review & editing [equal]), Eric Alberto Ocampo Batlle (Writing—review & editing [equal]), and Edson Da Costa Bortoni (Writing—review & editing [equal]).

Conflict of interest

The authors state that they have no known financial interests or personal relationships that could have potentially influenced the study presented in this paper.

Funding

This study did not receive funding from any public or private sector institution in Colombia, Peru, or Brazil.

References

1. Martinho G, Castro PJ, Santos P., Alves A, Araújo JMM, Pereiro AB Environmental behaviours and risk perception of domestic consumers: refrigeration equipment case study. *Clean Prod Lett* 2022;**3**:100024. https://doi.org/10.1016/j.clpl.2022.100024.
2. Aliane A, Abboudi S, Seladji C. *et al.* An illustrated review on solar absorption cooling experimental studies. *Renew Sustain Energy Rev* 2016;**65**:443–58. https://doi.org/10.1016/j.rser.2016.07.012.
3. Moayedi H, Yildizhan H, Aungkulanon P. *et al.* Green building's heat loss reduction analysis through two novel hybrid approaches. *Sustain Energy Technol Assess* 2023;**55**:102951. https://doi.org/10.1016/j.seta.2022.102951.
4. Assilzadeh F, Kalogirou SA, Ali Y. *et al.* Simulation and optimization of a LiBr solar absorption cooling system with evacuated tube collectors. *Renew Energy* 2005;**30**:1143–59. https://doi.org/10.1016/j.renene.2004.09.017.
5. Huang W, Marefati M. Energy, exergy, environmental and economic comparison of various solar thermal systems using water and Thermia Oil B base fluids, and CuO and Al2O3 nanofluids. *Energy Rep* 2020;**6**:2919–47. https://doi.org/10.1016/j.egyr.2020.10.021.
6. Liu W, Shen Y, Aungkulanon P. *et al.* Machine learning applications for photovoltaic system optimization in zero green energy buildings. *Energy Rep* 2023;**9**:2787–96. https://doi.org/10.1016/j.egyr.2023.01.114.
7. Fernandez-Garcia A, Zarza E, Valenzuela L. *et al.* Parabolic-trough solar collectors and their applications. *Renew Sustain Energy Rev* 2010;**14**:1695–721. https://doi.org/10.1016/j.rser.2010.03.012.
8. International Renewable Energy Agency (IRENA). *Solar Energy Data* 2024. https://www.irena.org/solar..

9. CSP.guru. *Plant list at*. https://csp.guru/ (2 April 2022, date last accessed).
10. Tzivanidis C, Bellos E, Antonopoulos KA. Energetic and financial investigation of a stand-alone solar-thermal Organic Rankine Cycle power plant. *Energ Conver Manage* 2016;**126**:421–33. https://doi.org/10.1016/j.enconman.2016.08.033.
11. Fan M, Liang H, You S. *et al.* Heat transfer analysis of a new volumetric based receiver for parabolic trough solar collector. *Energy* 2018;**142**:920–31. https://doi.org/10.1016/j.energy.2017.10.076.
12. Carrillo Caballero G, Escorcia YC, Sebasti L. *et al.* Thermal analysis of a parabolic trough collectors system coupled to an Organic Rankine Cycle and a two-tank thermal. *Energies* 2022;**15**:8261. https://doi.org/10.3390/en15218261.
13. Menni MBY, Chamkha AJ, Lorenzini G. *et al.* Advances of nanofluids in solar collectors—a review of numerical studies. *Math Model Eng Prob* 2019;**6**:415–27.
14. Menni HAY, Chamkha AJ. Advances of nanofluids in heat exchangers—a review. *Heat Trans* 2022;**48**:4321–49.
15. Padilla RV, Fontalvo A, Demirkaya G. *et al.* Exergy analysis of parabolic trough solar receiver. *Appl Therm Eng* 2014;**67**:579–86. https://doi.org/10.1016/j.applthermaleng.2014.03.053.
16. Allouhi A, Benzakour Amine M, Saidur R. *et al.* Energy and exergy analyses of a parabolic trough collector operated with nanofluids for medium and high temperature applications. *Energy Convers Manag* 2018;**155**:201–17.
17. Liang H, Fan M, You S. *et al.* Model development and performance analysis of the nanofluid-based direct absorption parabolic trough collectors. *J Clean Prod* 2018;**202**:299–310. https://doi.org/10.1016/j.jclepro.2018.08.119.
18. Menbari A, Alemrajabi AA, Rezaei A. Experimental investigation of thermal performance for direct absorption solar parabolic trough collector (DASPTC) based on binary nanofluids. *Exp Thermal Fluid Sci* 2017;**80**:218–27. https://doi.org/10.1016/j.expthermflusci.2016.08.023.
19. Heyhat MM, Valizade M, Abdolahzade S. *et al.* Thermal efficiency enhancement of direct absorption parabolic trough solar collector (DAPTSC) by using nanofluid and metal foam. *Energy* 2020;**192**:116662. https://doi.org/10.1016/j.energy.2019.116662.
20. Vasilescu C, Infante Ferreira C. Solar driven double-effect absorption cycles for sub-zero temperatures. *Int J Refrig* 2014;**39**:86–94. https://doi.org/10.1016/j.ijrefrig.2013.09.034.
21. Calise F. High temperature solar heating and cooling systems for different Mediterranean climates: dynamic simulation and economic assessment. *Appl Therm Eng* 2012;**32**:108–24. https://doi.org/10.1016/j.applthermaleng.2011.08.037.
22. Narayanan R, Harilal GK, Golder S. Feasibility study on the solar absorption cooling system for a residential complex in the Australian subtropical region. *Case Stud Therm Eng* 2021;**27**. 101202, https://doi.org/10.1016/j.csite.2021.101202.
23. Noferesti S, Ahmadzadehtalatapeh M, Motlagh VG. The application of solar integrated absorption cooling system to improve the air quality and reduce the energy consumption of the air conditioning systems in buildings—a full year model simulation. *Energy Build*. 2022;**274**.
24. Hadi Alaskaree E. Air conditioning of a classroom with solar energy using an absorptive cooling system. *Energ Buildings* 2023;**296**:113379. https://doi.org/10.1016/j.enbuild.2023.113379.
25. Sharma DK, Sharma D, Ali AHH. Optimization and thermoeconomic performance of a solar-powered vapor absorption cooling system integrated with sensible thermal energy storage. *Energ Conver Manage* 2023;**20**:100440. https://doi.org/10.1016/j.ecmx.2023.100440.
26. Gündüz Altiokka AB, Arslan O. Design and optimization of absorption cooling system operating under low solar radiation for residential use. *J Build Eng* 2023;**73**:106697. https://doi.org/10.1016/j.jobe.2023.106697.
27. Mehmood S, Lizana J, Friedrich D. Solar-driven absorption cooling system with latent heat storage for extremely hot climates. *Energ Conver Manage* 2023;**297**:117737. https://doi.org/10.1016/j.enconman.2023.117737.
28. Hakemzadeh MH, Sopian K, Kazem HA. *et al.* Evaluating the techno-economic viability of different solar collectors integrated into an adsorption cooling system in tropical climate conditions. *Sol Energy* 2024;**268**:112304. https://doi.org/10.1016/j.solener.2023.112304.
29. Messele Y, Assefa A. Thermal analysis, design and experimental investigation of parabolic trough solar collector. *Adv Intell Syst Comput* 2015;**334**:245–60. https://doi.org/10.1007/978-3-319-13572-4_20.
30. SLTL. Group. *Parabolic Trough Collector*. .
31. Enrique G, Caballero C. *Modelagem do comportamento integrado de um sistema de coletor cilíndrico parabólico operando com ciclo rankine orgânico e armazenamento térmico de dois tanques* 2018.
32. Forristall R. *Heat transfer analysis and modeling of a parabolic trough solar receiver implemented in engineering equation solver.* 2003. https://doi.org/NREL/TP-550-34169.
33. V. E. Dudley. *et al. Test results: SEGS LS-2 solar collector*. Albuquerque, NM, and Livermore, CA, 1994. https://doi.org/10.2172/70756.
34. Incropera FR, Dewitt D, Bergman T. *et al. Fundamentals of Heat and Mass Transfer*6th edn. Vol. 42007.
35. Gnielinski V. New equations for heat and mass transfer in turbulent pipe and channel flow. *Int Chem Eng* 1976;359–63.
36. Ratzel AC, Hickox CE, Gartling DK. Techniques for reducing thermal conduction and natural convection heat losses in annular receiver geometries. *J Heat Transfer* 1979;**101**:108. https://doi.org/10.1115/1.3450899.
37. Cengel Y. *Heat and Mass Transfer: A Practical Approach*3rd edn. McGraw Hill Book Company, 2006.
38. Touloukian Y, DeWitt D. *Engineering Heat Transfer*2nd edn. US, 2011.
39. Duffie JA, Beckman WA, Blair N. *Solar Engineering of Thermal Processes, Photovoltaics and Wind*5th edn. New Jersey: John Wiley & Sons, Inc, 2020.
40. Messele Y. *Thermal Analysis, Design and Experimental Investigation of Parabolic Trough Solar Collector. Master of Science in Mechanical Engineering*. Addis Ababa University, 2012.
41. Bellos E, Tzivanidis C, Tsimpoukis D. Thermal, hydraulic and exergetic evaluation of a parabolic trough collector operating with thermal oil and molten salt based nanofluids. *Energ Conver Manage* 2018;**156**:388–402. https://doi.org/10.1016/j.enconman.2017.11.051.
42. Chafie M, Ben Aissa MF, Guizani A. Energetic end exergetic performance of a parabolic trough collector receiver: an experimental study. *J Clean Prod* 2018;**171**:285–96. https://doi.org/10.1016/j.jclepro.2017.10.012.
43. Al-Oran O, Lezsovits F, Aljawabrah A. Exergy and energy amelioration for parabolic trough collector using mono and hybrid nanofluids. *J Therm Anal Calorim* 2020;**140**:1579–96. https://doi.org/10.1007/s10973-020-09371-x.
44. Bellos E, Tzivanidis C, Tsimpoukis D. Thermal, hydraulic and exergetic evaluation of a parabolic trough collector operating with thermal oil and molten salt based nanofluids. *Energ Conver Manage* 2018;**156**:388–402. https://doi.org/10.1016/j.enconman.2017.11.051.
45. Gomri R, Hakimi R. Second law analysis of double effect vapour absorption cooler system. *Energ Conver Manage* 2008;**49**:3343–8. https://doi.org/10.1016/j.enconman.2007.09.033.
46. Gebreslassie BH, Medrano M, Boer D. Exergy analysis of multi-effect water-LiBr absorption systems: from half to triple effect. *Renew Energy* 2010;**35**:1773–82. https://doi.org/10.1016/j.renene.2010.01.009.
47. Bellos E, Tzivanidis C, Pavlovic S. *et al.* Thermodynamic investigation of LiCl-H2O working pair in a double effect absorption chiller driven by parabolic trough collectors. *Thermal Sci Eng Prog* 2017;**3**:75–87. https://doi.org/10.1016/j.tsep.2017.06.005.

48. Dincer I, Rosen MA. 2021, ch. 8. Exergy analyses of absorption cooling systems. In *Exergy*3rd edn. Elsevier Science. 143–65.
49. Domínguez-Inzunza LA, Hernández-Magallanes JA, Sandoval-Reyes M. *et al.* Comparison of the performance of single-effect, half-effect, double-effect in series and inverse and triple-effect absorption cooling systems operating with the NH3–LiNO3 mixture. *Appl Therm Eng* 2014;**66**:612–20. https://doi.org/10.1016/J.APPLTHERMALENG.2014.02.061.
50. Lawan S. *Thermodynics analysis of single and series flow double effect solar assisted absorption refrigeration systems using LiBr-H2O working pairs*. Master Thesis. Cyprus International University, 2018.
51. Bellos E, Tzivanidis C, Pavlovic S. *et al.* Thermodynamic investigation of LiCl-H2O working pair in a double effect absorption chiller driven by parabolic trough collectors. *Thermal Sci Eng Prog* 2017;**3**:75–87. https://doi.org/10.1016/j.tsep.2017.06.005.
52. Dincer I, Rosen MA. 2021, ch. 8. Exergy analyses of absorption cooling systems. In *Exergy*3rd edn. Elsevier Science. 143–65.
53. Lawan S. *Thermodynics analysis of single and series flow double effect solar assisted absorption refrigeration systems using LiBr-H2O working pairs*. Master Thesis. Cyprus International University, 2018.
54. E. Environmental Protection Agency. *Basic information of air emissions factors and quantification*. 2024.
55. International Energy Agency. *Emission factor for greenhouse gas inventories*. 2017.
56. Marif Y, Benmoussa H, Bouguettaia H. *et al.* Numerical simulation of solar parabolic trough collector performance in the Algeria Saharan region. *Energ Conver Manage* 2014;**85**:521–9. https://doi.org/10.1016/j.enconman.2014.06.002.
57. García-Valladares O, Velázquez N. Numerical simulation of parabolic trough solar collector: improvement using counter flow concentric circular heat exchangers. *Int J Heat Mass Transf* 2009;**52**:597–609. https://doi.org/10.1016/j.ijheatmasstransfer.2008.08.004.
58. Marif Y, Benmoussa H, Bouguettaia H. *et al.* Numerical simulation of solar parabolic trough collector performance in the Algeria Saharan region. *Energ Conver Manage* 2014;**85**:521–9. https://doi.org/10.1016/j.enconman.2014.06.002.
59. García-Valladares O, Velázquez N. Numerical simulation of parabolic trough solar collector: improvement using counter flow concentric circular heat exchangers. *Int J Heat Mass Transf* 2009;**52**:597–609. https://doi.org/10.1016/j.ijheatmasstransfer.2008.08.004.
60. Yılmaz İH, Saka K, Kaynaklı Ö. *et al.* Performance assessment and solution procedure for series flow double-effect absorption refrigeration systems under critical operating constraints. *Arab J Sci Eng* 2019;**44**:5997–6011. https://doi.org/10.1007/s13369-019-03805-x.
61. Garousi Farshi L, Seyed Mahmoudi SM, Rosen MA. Analysis of crystallization risk in double effect absorption refrigeration systems. *Appl Therm Eng* 2011;**31**:1712–7. https://doi.org/10.1016/j.applthermaleng.2011.02.013.
62. Yılmaz İH, Saka K, Kaynaklı Ö. *et al.* Performance assessment and solution procedure for series flow double-effect absorption refrigeration systems under critical operating constraints. *Arab J Sci Eng* 2019;**44**:5997–6011. https://doi.org/10.1007/s13369-019-03805-x.
63. Garousi Farshi L, Seyed Mahmoudi SM, Rosen MA. Analysis of crystallization risk in double effect absorption refrigeration systems. *Appl Therm Eng* 2011;**31**:1712–7. https://doi.org/10.1016/j.applthermaleng.2011.02.013.
64. Rosales-Pérez JF, Villarruel-Jaramillo A, Pérez-García M. *et al.* Techno-economic analysis of hybrid solar thermal systems with flat plate and parabolic trough collectors in industrial applications. *Alex Eng J* 2024;**86**:98–119. https://doi.org/10.1016/j.aej.2023.11.056.
65. Bellos E, Chatzovoulos I, Tzivanidis C. Yearly investigation of a solar-driven absorption refrigeration system with ammonia-water absorption pair. *Therm Sci Eng Pro* 2021;**23**:100885. https://doi.org/10.1016/j.tsep.2021.100885.
66. Moraga-Contreras C, Cornejo-Ponce L, Vilca-Salinas P. *et al.* Evolution of solar energy in Chile: residential opportunities in Arica and Parinacota. *Energies* 2022;**15**:551. https://doi.org/10.3390/en15020551.
67. Quiñones G, Felbol C, Valenzuela C. *et al.* Analyzing the potential for solar thermal energy utilization in the Chilean copper mining industry. *Sol Energy* 2020;**197**:292–310. https://doi.org/10.1016/j.solener.2020.01.009.
68. Metodología para la determinación del precio de bolsa propuestas de ajuste temporal. 1299. 2023
69. Liang H, Han H, Wang F. *et al.* Experimental investigation on spectral splitting of photovoltaic/thermal hybrid system with two-axis sun tracking based on SiO2/TiO2 interference thin film. *Energ Conver Manage* 2019;**188**:230–40. https://doi.org/10.1016/j.enconman.2019.03.060.

International Journal of Low-Carbon Technologies, 2025, 20, 940–956
https://doi.org/10.1093/ijlct/ctae142
Original Article